INTL JOURNAL OF ELECTRONICS AND TELECOMMUNICATIONS, 2021, VOL. 67, NO. 3, PP. 445-450
Manuscript received December 30, 2020; revised July, 2021 DOI: 10.24425/ijet.2021.137832

Asynchronous Demodulation Method for Four SSB arranged on Frequency Axis in Mobile Radio Path using Hilbert Transform

Kazuhiro Daikoku

Abstract—**In this paper, an asynchronous demodulation method for a four-single sideband (SSB) signal arranged on the frequency axis is developed to support burst mode transmission in a mobile radio path and to achieve greater data throughputs. When a reduced pilot carrier is placed at the center of the 4-SSB signal, it is guarded by lower and upper sidebands, that is, this scheme is classified into a tone-in-band (TIB) system. Digital signal processing (DSP) processors are useful for implementing a Hilbert transform. However, we have for a long time neglected introducing it into the demodulation process of SSB signals.**

Keywords—**asynchronous demodulation, 4-SSB, ISB, mobile radio path, Hilbert transform, HF/VHF band telecommunications, tactical communications, underwater communications**

I. Introduction

THE conventional method for demodulating SSB (single sideband) signals propagating through fading environments makes full use of a low level pilot tone along with the SSB signal, which is used for an AGC (automatic gain control) and an AFC (automatic frequency control) including a PLL (phase lock loop) to combat severe fading. However, it is difficult to achieve a practically perfect AGC and AFC/PLL performance for the pilot signal contaminated by fading in an SSB receiver [1].

We have developed asynchronous demodulation methods for an RZ SSB (real zero SSB) signal in two phases, that utilizes neither AGC nor AFC/PLL to combat severe fading. In the first phase, an RZ SSB receiver for land mobile services was fabricated using discrete analogue components [2]. Further, we took part in field tests to demonstrate that the RZ SSB receiver is effective for digital data communications in standard 3kHz HF (high frequency) channel allocations [3]. During the field tests, two-branch space diversity reception with an equal-gain combining method was utilized to improve the quality of received signals. Consequently, a bit error rate (BER) performance through an HF radio channel was first investigated using both RZ SSB transceivers and an ITU-T (International Telecommunication Union Telecommunication Standardization Sector) V.29 modem (MOdulator-DEModulator, a modem is the product of NEC), whose data transmission rates range from 2.4 to 9.6kbit/s. Successful results on the BER performance encouraged us to try JPEG (Joint Photo graphic Expert Group)/text file transmission, and to develop a suitable communication protocol for a simplex HF radio channel. As the RZ SSB transceiver is able to support burst mode transmission we employed a fall back mode and an automatic repeat request (ARQ) to improve communication quality with modifying an ITU-T T.30 protocol. JPEG/text files have been transmitted between two coastal stations approximately 2000 km apart through an HF radio path by switching between transmission and reception just like in ping-pong transmission [3].

As the RZ SSB receiver using discrete analogue components possesses the threshold effect in a low input signal power region, in the second phase we implemented the RZ SSB receiver based on DSP (digital signal processing) processors to remove the threshold effect [4]. This is because analogue circuits cannot cope with the mathematical calculations. In contrast, DSP processors make it possible to use Hilbert transform [5], whose technical potential for demodulation of SSB signals has been ignored for a long time. As a Hilbert transformer, which exhibits a linear phase response, is required for the signal processing, finite impulse response (FIR) Hilbert transformers use dedicated hardware with DSP processors used to implement their algorithms. DSP processors and/or general-purpose processors are continually being improved with costs coming down every year and performance always increasing. We achieved an asynchronous demodulation method for the RZ SSB signal without the threshold effect using DSP processors. We performed transmission experiments to demonstrate effectiveness of the present signal processing using voiceband modems such as ITU-T V.29 16QAM with a data transmission rate of 16kbps, ITU-T V.32 bis 64/128QAM with that of 14.4kbps, and V.32 bis 256QAM with that of 19.2kbps [6] (modems are the product of NEC) in AWGN (additive white Gaussian noise) and flat Rayleigh fading environments.

The developed asynchronous demodulation method may be extended to a 4-SSB signal based on an ISB (independent sideband) scheme, which appears to offer potential for much greater throughputs for tactical communication systems [7,8], underwater communications [9] and so on. When a reduced pilot carrier is placed at the center of the 4-SSB signal, it is easy to insert a pilot carrier without reducing the baseband signal spectrum in a USB (upper sideband) and a LSB (lower sideband). Moreover, due to high correlation between the fades experienced by the pilot carrier and the baseband signals in USBs and LSBs, a tone-in-band (TIB) system makes it possible to bring a high quality of demodulated signals [10]. In the next section, we describe how to construct the 4-SSB signal and how to asynchronously demodulate the 4-SSB signal in detail.

Author is retired, Tokyo, Japan (e-mail: kdaikoku@rk9.so-net.ne.jp).

II. ASCYNCHRONOUS DEMODULATION METHOD

A. Transmitted signal

The transmitted signal of a 4-SSB system based on an ISB scheme, whose channel arrangement on the frequency axis is depicted in Fig. 1, can be described with the complex envelope as follows:

$$f(t) = P + (a(t) - j\mathrm{H}[a(t)]) + (b(t) + j\mathrm{H}[b(t)]) + \\ +(c(t) - j\mathrm{H}[c(t)])\exp(-j\omega_s t) + \\ +(d(t) + j\mathrm{H}[d(t)])\exp(j\omega_s t). \quad (1)$$

where $a(t)$, $b(t)$, $c(t)$ and $d(t)$ are mutually independent baseband signals for the first, second, third and fourth channel, respectively. H[$y(t)$] is the Hilbert transform of $y(t)$. From the nature of the Hilbert transform, HH[$y(t)$] becomes -$y(t)$ [5]. P is a pilot carrier component located at the zero-frequency whose level is large enough to use the received signal strength indication (RSSI) in a receiver. Complex sub-carriers of $\exp(-j\omega_s t)$ and $\exp(j\omega_s t)$ are respectively used to set the LSB with $c(t)$ and the USB with $d(t)$ at an appropriate frequency position. $\omega_s(=2\pi f_s)$ is the angular frequency, in the case of Fig. 1, f_s=3.0/3.4kHz.

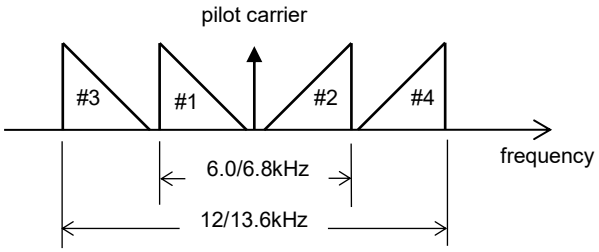

Fig. 1. Channel arrangement of 4-SSB scheme on the frequency axis.

B. Mobile radio path

Figure 2 illustrates a propagation path model from a transmitter to a receiver with the complex envelope for the 4-SSB with reduced-pilot carrier signal. For convenience, the complex baseband signals are indicated with double lines. When the transmitted signal is fed into fading channel, it is affected by multiplicative fading noise. At the receiver, thermal noise is added to the signal. Then, the received signal is given by

$$r(t) = c_{cg}(t) f(t) + n(t), \quad (2)$$

where $n(t)$ is additive white Gaussian noise (AWGN) with the power spectral density of n_0 in both the real and imaginary components. The channel's complex gain $c_{cg}(t)$ incorporates both fading noises and frequency offset between the transmitter and the receiver as

$$c_{cg}(t) = g_{cg}(t)\exp j\Delta\omega_0 t, \quad (3)$$

where $\Delta\omega_0 = 2\pi f_0$, and f_0 is the residual frequency offset, which is determined from the frequency stability of oscillators installed in both the transmitter and the receiver.

The power spectrum of the complex gain is described by a U-shaped spectrum, whose central frequency in this model is f_0 [1]. The overall bandwidth is twice the maximum Doppler frequency, f_D, which is calculated as $f_D = 9.25 \times 10^{-4} f_{RF} v$, where f_{RF} is the radio frequency in MHz and v is the maximum vehicular speed in km/h. For example, when f_{RF} =30 MHz and v =100km/h, f_D =2.8Hz.

On the basis of the statistical model of flat Rayleigh fading and the implementation of its simulator [1], the time function $g_{cg}(t)$ can be expressed as

$$g_{cg}(t) = \alpha(t)\exp j\varphi(t).$$

Here, the amplitude variation $\alpha(t)$ is statistically governed by the Rayleigh distribution. The function $\varphi(t)$ is described by the uniform distribution, that is, random phase noise. It is noted that the dynamic range of flat Rayleigh fading is relatively wide.

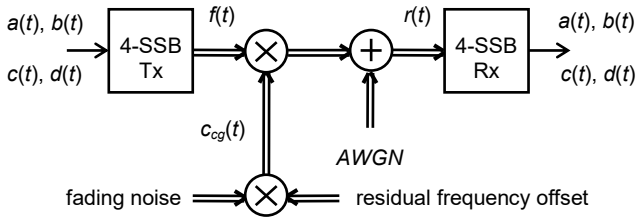

Fig. 2. Propagation path model from 4-SSB Tx to Rx with complex baseband representation.

C. Receiver signal processing

Figure 3 shows a schematic diagram of an asynchronous demodulation circuit for a 4-SSB system. The received signal $r(t)$ with the complex envelope can be calculated from (1-3) when the power of $c_{cg}(t)f(t)$ is much larger than that of $n(t)$.

$$r(t) = \alpha(t)\{P + (a(t) - j\mathrm{H}[a(t)]) + (b(t) + j\mathrm{H}[b(t)]) + \\ +(c(t) - j\mathrm{H}[c(t)])\exp(-j\omega_s t) + \\ +(d(t) + j\mathrm{H}[d(t)])\exp(j\omega_s t)\}\exp j(\Delta\omega_0 t + \varphi(t)). \quad (4)$$

Referring to the signal flow depicted in Fig.3, we have a demodulation procedure which is described in the following steps:

Step 1: Extracting the pilot carrier component from (4) using a proper narrowband finite impulse response low-pass filter (FIR-LPF #1), whose cut-off frequency is narrow enough to extract the pilot carrier, we have

$$r_{nb}(t) = P\alpha(t)\exp j(\Delta\omega_0 t + \varphi(t)). \quad (5)$$

Note that the passband ripples of FIR-LPF#1 should be as small as possible.

Step 2: Substituting the pilot carrier component of (5) from (4) as much as possible, we have

$$r_r(t) = \alpha(t)\{(a(t) - j\mathrm{H}[a(t)]) + (b(t) + j\mathrm{H}[b(t)]) + \\ +(c(t) - j\mathrm{H}[c(t)])\exp(-j\omega_s t) +$$

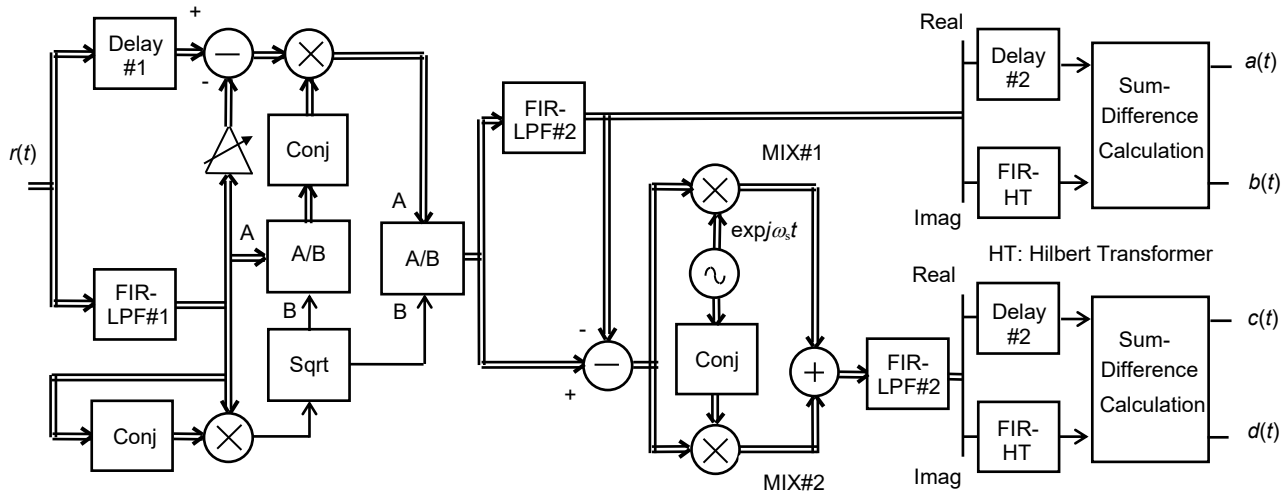

Fig. 3. Schematic diagram of asynchronous demodulation circuit for 4-SSB system.

$$+(d(t)+j\mathrm{H}[d(t)])\exp(j\omega_s t)\}\exp j(\Delta\omega_0 t+\varphi(t)). \quad (6)$$

Delay #1 in Fig. 3 is introduced for the input signal of $r(t)$ to compensate for the delay time introduced by the narrowband FIR-LPF #1. For simplicity, we neglect the delay associated with the narrowband FIR-LPF #1 in the mathematical formulation.

Step 3: Multiplying (5) by the complex conjugate of (5) and taking the square root, we obtain the degenerated envelope,

$$r_{da}(t)=\sqrt{r_{nb}(t)r_{nb}^{*}(t)}= \\ =P\alpha(t), \quad (7)$$

where $y^*(t)$ denotes the complex conjugate of $y(t)$.

Step 4: Dividing (5) by (7), we get

$$r_{pp}(t)=r_{nb}(t)/r_{da}(t)= \\ =\exp j(\Delta\omega_0 t+\varphi(t)). \quad (8)$$

This is the complex phase angle of the residual frequency offset-plus-random phase noise.

Step 5: Multiplying (6) with the complex conjugate of (8) to cancel out the residual frequency offset-plus-random phase noise caused by fading, we have

$$r_{rp}(t)=r_r(t)r_{pp}^{*}(t)= \\ =\alpha(t)\{(a(t)-j\mathrm{H}[a(t)])+(b(t)+j\mathrm{H}[b(t)])+ \\ +(c(t)-j\mathrm{H}[c(t)])\exp(-j\omega_s t)+ \\ +(d(t)+j\mathrm{H}[d(t)])\exp(j\omega_s t)\}. \quad (9)$$

Step 6: Dividing (9) by (7), we obtain

$$r_{rd}(t)=r_{rp}(t)/r_{da}(t)= \\ =\{(a(t)-j\mathrm{H}[a(t)])+(b(t)+j\mathrm{H}[b(t)])+ \\ +(c(t)-j\mathrm{H}[c(t)])\exp(-j\omega_s t)+ \\ +(d(t)+j\mathrm{H}[d(t)])\exp(j\omega_s t)\}/P. \quad (10)$$

We may put P=1 in the following steps without loss of generality.

Step 7: FIR-LPF #2, whose cut-off frequency is f_s, is used for (10) to extract the following signal, that is,

$$r_{ab}(t)=a(t)-j\mathrm{H}[a(t)]+b(t)+j\mathrm{H}[b(t)]= \\ =a(t)+b(t)-j\mathrm{H}[a(t)-b(t)]. \quad (11)$$

Note that the passband ripples of FIR-LPF #2 should be as small as possible.

Step 8: Introducing the real and the imaginary parts of (11) into Delay #2 and FIR-Hilbert transformer with the filter length of N, respectively, we get

$$r_{dab}(t)=a(t-\tau)+b(t-\tau), \quad (12)$$

$$r_{hab}(t)=a(t-\tau)-b(t-\tau). \quad (13)$$

where τ is the delay time equivalent to the delay time generated by the FIR-Hilbert transformer, whose value corresponds to $N/2$. Note that the present Hilbert transformer works only for even orders. Here, we use the following relation [5], that is,

$$\mathrm{HH}[y(t)]=-y(t). \quad (14)$$

Step 9: Decomposing (12) and (13) using the sum/difference calculation circuit, we finally obtain the first and second channel signal

$$(r_{dab}(t)+r_{hab}(t))/2=a(t-\tau), \\ (r_{dab}(t)-r_{hab}(t))/2=b(t-\tau).$$

Note that the perfect channel separation can be performed by the ideal Hilbert transformer with no amplitude ripple. Hence, a channel separation performance due to amplitude ripples of FIR-Hilbert transformer will be discussed in the next section.

Step 10: Substituting (11) from (10), we get the following signals, that is,

$$r_{scd}(t)=(c(t)-j\mathrm{H}[c(t)])\exp(-j\omega_s t)+ \\ +(d(t)+j\mathrm{H}[d(t)])\exp(j\omega_s t)\}. \quad (15)$$

Step 11: First, multiplying (15) by the oscillator output of $\exp(j\omega_s t)$ using MIX #1, we obtain

$$r_{lcd}(t) = r_{scd}(t) \times \exp(j\omega_s t) = \\ = c(t) - j\mathrm{H}[c(t)] + (d(t) + jHd(t)]) \exp(j2\omega_s t). \quad (16)$$

Then, multiplying (15) by the oscillator output of $\exp(-j\omega_s t)$ using MIX #2, we have

$$r_{ucd}(t) = r_{scd}(t) \times \exp(-j\omega_s t) = \\ = (c(t) - jH[c(t)] \exp(-j2\omega_s t) + d(t) + j\mathrm{H}[d(t)]. \quad (17)$$

Adding the two output signals, i.e., (16) and (17), we get the following signal after filtering with FIR-LPF #2, whose cut-off frequency is f_s, that is,

$$r_{cd}(t) = c(t) - j\mathrm{H}[c(t)] + d(t) + j\mathrm{H}[d(t)] = \\ = c(t) + d(t) - j\mathrm{H}[c(t) - d(t)]. \quad (18)$$

Step 12: Introducing the real and the imaginary parts of (18) into Delay #2 and FIR-Hilbert transformer with the filter length of N, respectively, we get

$$r_{dcd}(t) = c(t-\tau) + d(t-\tau), \quad (19)$$
$$r_{hcd}(t) = c(t-\tau) - d(t-\tau). \quad (20)$$

where τ is the delay time corresponding to the delay time generated by the FIR-Hilbert transformer, whose value corresponds to $N/2$. Note that the present Hilbert transformer works only for even orders.

Step 13: Decomposing (19) and (20) using the sum/difference calculation circuit, we finally obtain the third and fourth channel signal,

$$(r_{dcd}(t) + r_{hcd}(t)) / 2 = c(t-\tau),$$
$$(r_{dcd}(t) - r_{hcd}(t)) / 2 = d(t-\tau).$$

A channel separation issue due to amplitude ripples of FIR-Hilbert transformers will be discussed in the next section.

D. Channel separation performance

The 4-SSB signal can be converted into the 2-ISB signal in the demodulation process, i.e., (11) and (18)

$$r_{ab}(t) = a(t) + b(t) - j\mathrm{H}[b(t) - b(t)],$$
$$r_{cd}(t) = c(t) + d(t) - j\mathrm{H}[c(t) - d(t)].$$

Taking the real part of the above equations, we get the sum signals, i.e., $a(t)+b(t)$ and $c(t)+d(t)$. Hilbert-transforming the imaginary part of the above equations using the ideal Hilbert transform of (14), we get the difference signals, i.e., $a(t)$-$b(t)$ and $c(t)$-$d(t)$. Then, transmitted baseband signals $a(t)$ and $b(t)$ are resolved from the sum and the difference equation using a sum-difference calculation circuit. $c(t)$ and $d(t)$ are also resolved with the same procedure.

As the ideal Hilbert transformer cannot be realized, we take Hilbert transformers designed either as FIR or as IIR (infinite impulse response) digital filters. We choose FIR-Hilbert transformers from the following reasons, although FIR filters are a higher complexity compared with the corresponding IIR filters. FIR-Hilbert transformers can have exact linear phase and their stability is guaranteed. Moreover, they are less sensitive to the coefficients rounding and their phase response is not affected by this rounding. However, for a small transition bandwidth and a small passband ripple the resulting Hilbert transformer requires a very high length.

The design of optimum equiripple FIR Hilbert transformers is usually performed by Parks-McClellan algorithm. Channel separation performance characteristics should be examined using MATLAB, where the sampling frequency of 8kHz is used for the baseband signal whose spectrum is ranging from 300 to 3400Hz. The channel separation is equivalent to a crosstalk, an adjacent channel interference (ACI) and an intersymbol interference (ISI) for analogue and/or digital signals.

1) For analogue signals

In the case of an ISB channel which transmits and receives analogue signals such as voice/speech/music signals, we understand that a high separation level may be required considering human perception ability. This is because voice/speech/music signals possess relatively wide dynamic range.

Figure 4 indicates the passband ripples generated from the transition bandwidth of B_t=4.5% and the length of N=82. Using this FIR-Hilbert transformer, we may estimate on the channel separation performance as shown in Fig. 5, where the channel separation is more than 60 dB in the frequency range from 180 to 3820Hz, that is, the transition bandwidth of B_t=4.5%.

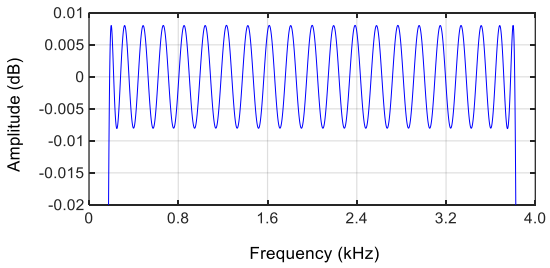

Fig. 4. Passband amplitude ripples for B_t=4.5% and N=82.

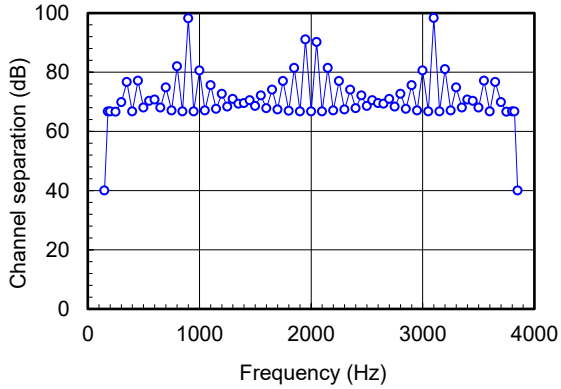

Fig. 5. Channel separation performance for analogue signal.

2) For digital signal

In the case of digital signals such as a QAM (quadrature amplitude modulation) scheme used in an ITU-T voiceband modem, we may take into consideration that digital signals possess strong immunity against interference, compared with analogue signals. A required channel separation level may be estimated referring to results on EBR vs. C/I_c (power ratio of the desired signal to the co-channel interference). The computer simulation results on BER vs. C/I_c performance for QPSK (quadrature phase shift keying), 16 QAM and 64QAM with a maximal ratio combining space diversity in Rayleigh fading environments were reported in [11]. Taking the required C/I_c of 30dB, we can estimate the BER of $1.5\cdot10^{-6}$, $6\cdot10^{-5}$ and $4\cdot10^{-4}$ for QPSK, 16QAM and 64QAM, respectively. We adopt the required C/I_c of 30dB to a tentative target for channel separation performance.

To obtain the channel separation of 30dB, we simulate using the FIR-Hilbert transformer with the parameters of B_t=4.5% and N=32. Figure 6 is the simulated result on the passband ripples performance of the FIR-Hilbert transformer. Figure 7 is the simulated results on the channel separation performance, where the channel separation obtains at least 30 dB in the frequency range from 180 to 3820Hz, that is, the transition bandwidth of B_t=4.5%.

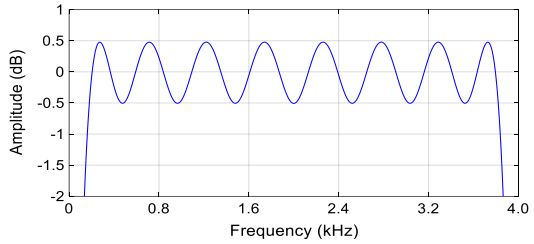

Fig. 6. Passband amplitude ripples for B_t=4.5% and N=32.

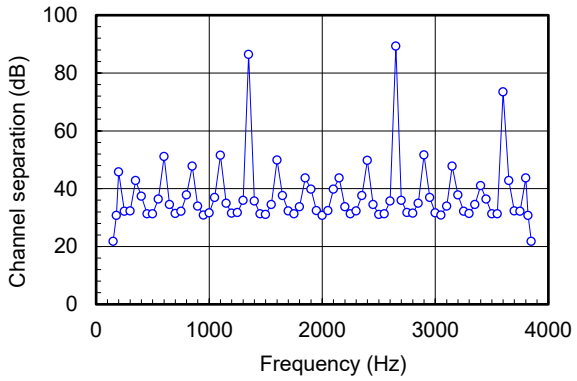

Fig.7. Channel separation performance for digital signal.

III. DISCUSSIONS

1) Orthogonal four-SSB scheme

An orthogonal 4-SSB scheme, where two ISB signals are orthogonally multiplexed on the same complex frequency band of ISB, was proposed to increase the spectrum efficiency of SSB in [12-15]. The modulated signal of an orthogonal 4-SSB $S(t)$ is described in the complex envelope using baseband signals such as $a(t)$, $b(t)$, $c(t)$ and $d(t)$, where an ISB #1 and an ISB #2 are respectively composed of $a(t)$ and $b(t)$, and $c(t)$ and $d(t)$ with the same carrier frequency of zero, then, the ISB #1 and the ISB #2 are arranged so that they are orthogonal [13] as follows:

$$\begin{aligned} S(t) &= (a(t) - j\mathrm{H}[a(t)]) + (b(t) + j\mathrm{H}[b(t)]) + \\ &+ j\{(c(t) - j\mathrm{H}[c(t)]) + (d(t) + j\mathrm{H}[d(t)])\} = \\ &= a(t) + b(t) + \mathrm{H}[c(t)] - \mathrm{H}[d(t)] + \\ &+ j(-\mathrm{H}[a(t)] + \mathrm{H}[b(t)] + c(t) + d(t). \end{aligned} \tag{21}$$

where the ISB in the first line and the second line of (21) are located on the real axis and the imaginary axis, respectively. The real and the imaginary part of (21) are respectively written as $S_I(t)$ and $S_Q(t)$, that is,

$$S_I(t) = a(t) + b(t) + \mathrm{H}[c(t)] - \mathrm{H}[d(t)], \tag{22}$$

$$S_Q(t) = -\mathrm{H}[a(t)] + \mathrm{H}[b(t)] + c(t) + d(t). \tag{23}$$

Here, $S_I(t)$ and $S_Q(t)$ are the in-phase and the quadrature component of the modulated signal, respectively, which are used in signal processing for demodulation.

When the transmitted signal expressed by (21) is demodulated in an orthogonal 4-SSB receiver, we obtain the following demodulated signals through the ideal Hilbert transform using the in-phase and the quadrature signal, i.e., $S_I(t)$ and $S_Q(t)$

$$\begin{aligned} q_{LSB}(t) &= \frac{1}{2}\{(S_I(t) + \mathrm{H}[S_Q(t)]) + j(S_Q(t) - \mathrm{H}[S_I(t)])\} = \\ &= (a(t) + \mathrm{H}[c(t)]) + j(c(t) - \mathrm{H}[a(t)]) = \\ &= (a(t) - j\mathrm{H}[a(t)]) + j(c(t) - j\mathrm{H}[c(t)]). \end{aligned} \tag{24}$$

$$\begin{aligned} q_{USB}(t) &= \frac{1}{2}\{(S_I(t) - \mathrm{H}[S_Q(t)]) + j(S_Q(t) + \mathrm{H}[S_I(t)])\} = \\ &= (b(t) - \mathrm{H}[d(t)]) + j(d(t) + \mathrm{H}[b(t)]) = \\ &= (b(t) + j\mathrm{H}[b(t)]) + j(d(t) + j\mathrm{H}[d(t)]). \end{aligned} \tag{25}$$

Equations (24) and (25) are corresponding to the LSB and the USB of the orthogonal 4-SSB signal of (21), respectively. It is not surprising that (24) and (25) possess inherently a strong Hilbert-transformed ACI (on analogue signal) or ISI (on digital signal) in the desired channel caused by the orthogonal arrangement of two ISB signals. Then, we discuss the influence of the terms in demodulation process on analogue and digital signals.

On analogue signals:

The demodulated signals, i.e., (24) and (25), indicate that their real part is connected with their imaginary part through the Hilbert transform as follows:

$$\mathrm{H}[a(t) + \mathrm{H}[c(t)]] = -(c(t) - \mathrm{H}[a(t)]).$$

$$\mathrm{H}[b(t) - \mathrm{H}[d(t)]] = d(t) + \mathrm{H}[b(t)].$$

The above first equation indicates that a single governing equation for $a(t)$ and $c(t)$ is only provided from the demodulation process. However, two governing equations for $a(t)$ and $c(t)$ are required to analytically solve $a(t)$ and $c(t)$. The same is true for $b(t)$ and $d(t)$. Therefore, there is no way to remove the ACI from (24) and (25). As a result, it is impossible to introduce the orthogonal 4-SSB scheme into voice/speech/music communications using analogue signals.

On digital signals:

Nevertheless, there is a certain way to reduce an adverse effect of the ISI in an orthogonal 4-SSB combined with a QPSK or a QAM scheme. If H[$a(t)$]/H[$c(t)$] in (24) and H[$b(t)$]/H[$d(t)$] in (25) can be minimized by some of digital techniques, $a(t)+jc(t)$ and $b(t)+jd(t)$ may be applicable to transmit modulated signals, for example, QAM #1 and QAM #2, whose signals are written by the in-phase and the quadrature components [14]. Various techniques such as a turbo equalizer, a soft-canceller (SC)/simplified-minimum square error (S-MMSE) type equalizer, a soft-input soft-output (SISO) equalizer, shadow equalizer and so on have been studied to decrease the influence of the ISI [14-16]. However, it may take some time for an ultimate solution with low complexity to diminish the ISI.

When an orthogonal 4-SSB is utilized in a stand-alone system, there is another issue that a synchronous demodulation method is required.

2) Four-SSB scheme on the frequency axis

Signal processing from Step 1 to 6 is devoted to eliminating amplitude variation and random noise caused by fading plus the residual frequency offset. It is demonstrated in [4] that this signal processing is effective not only to combat severe fading but also to produce an excellent result on asynchronous demodulation of the RZ SSB signal. Then, we introduce the same signal processing to an asynchronous demodulation for a 4-SSB signal. The succeeding process from Step 7 to 13 is devoted to demodulating four baseband signals using Hilbert transformers. Referring to (11) and (18) in the previous section, there is no adjacent channel interference. Then, this scheme can be surely applicable to analogue and/or digital signals. This is because the present 4-SSB scheme is arranged on the frequency axis although the spectrum efficiency is not improved, as compared with the orthogonal 4-SSB scheme.

IV. Conclusion

In this paper, we demonstrate how to implement an asynchronous demodulation method using DSP processors into a 4-SSB receiver, which can support burst mode transmission. This method for 4-SSB, that is, 2-ISB can be easily applicable to ISB signal. As the proposed 4-SSB system with a reduced pilot carrier which is located at the center of the modulated signal is categorized into a TIB system, the 4-SSB system brings excellent communication quality even in severe fading environments and makes it possible not only to increase data throughputs but also to expand the application range of the mobile radio services in the HF as well as the VHF band.

References

[1] W. C. Jakes, Ed., *Microwave Mobile Communications*, IEEE Press, 1993, ISBN 0-7803-1069-1

[2] K. Daikoku and K. Suwa, “RZ SSB transceiver with equal-gain combiner for speech and data transmission,” *Proc. IEEE GLOBECOM’88*, Hollywood, FL, USA, pp.26.4.1-26.4.5, 1988, DOI: 10.1109/GLOCOM.1988.25953

[3] K. Daikoku, “Field test results on JPEG/text file transmission employing RZ SSB transceivers through HF radio channels,” *IEE Proc. Communi*., vol. 151, no. 1, pp.50-58, 2004, DOI: 10.1049/ip-com:20040347

[4] K. Daikoku, “Hilbert transform applications in asynchronous demodulation for real zero single sideband signals in mobile radio path,” *J. Signal Process.*, vol. 25, no. 1, pp. 11–24, Jan. 2021. DOI: 10.2299/jsp.25.11.

[5] S. L. Hahn, *Hilbert Transforms in Signal Processing*, Artech House, 1996, ISBN 0-9006-886-0

[6] W. T. Webb and L. Hanzo, *Modern Quadrature Amplitude Modulation*, Pentech Press, 1994, ISBN 0-7273-1701-6

[7] N. C. Davies, “Digital radio and its application in HF (2-30 MHz) band,” *Doctor Thesis to the University of Leeds*, May 2004.

[8] R. C. Daniels and S. W. Peters, “A new MIMO HF data link: Designing for high data rates and backwards compatibility,” *2013 IEEE MILCOM*, San Diego, CA, USA, pp.1-6, 2013, DOI: 10.1109/MILCOM.2013.214

[9] M. Kuzlu, H. Dinçer and S. Öztürk, “DSP implementation of underwater communication using SSB modulation with random carrier frequencies,” *Sci. Res. Essays,* vol. 5, no. 10, pp.1084-1099, 2010, ISSN 1992-2248

[10] T. S. Rappaport, *Wireless Communications*, Prentice Hall, 1996, ISBN 0-13-461088

[11] S. Sampei, S. Komaki and N. Morinaga, “Adaptive modulation/TDMA scheme for large capacity personal multi-media communication systems,” *IEICE Trans. Communi*., vol. E77-B, no. 9 pp.1096-1103, 1994.

[12] G. Ohta, M. Nanri, M. Uesugi, T. Sato, H. Tominaga, “A study of new modulation method consisted of orthogonal four SSB elements having a common carrier frequency,” *The 11th International Symposium on Wireless Personal Multimedia Communications (WPMC 2008)*, Lapland, Finland, 8–11 Sep. 2008.

[13] M. Nanri, “Transmitter and SSB signal generation method,” US Patent Application Publication, Pub. No.: US 2010/0246710 A1, Pub. Date: Sep. 30, 2010.

[14] A. M. Mustafa, Q. N. Nguyen, T. Sato and G. Ohta, “Four single-sideband M-QAM modulation using soft input soft output equalizer over OFDM,” *2018 28th International Telecommunication Networks and Applications Conference (ITNAC),* Sydney, NSW, Australia, 21-23 Nov. 2018, DOI: 10.1109/ATNAC.2018.8615451

[15] M. M. Alhasani, Q. N. Nguyen, G. Ohta, and T. Sato, “A novel four single-sideband M-QAM modulation scheme using a shadow equalizer for MIMO system toward 5G communications,” *Sensors*, 2019, 9, 1944; DOI:10.3390/s19081944

[16] B. Pitakdumrongkija, H. Suzuki, S. Suyama and K. Fukawa, "Single sideband QPSK with turbo equalization for mobile communications," *2005 IEEE 61st VTC’05*, Stockholm, Sweden, pp. 538-542, 30 May-1 June 2005, DOI: 10.1109/VETECS.2005.1543349